Two-temperature nonequilibrium molecular dynamics simulation of thermal transport across metal-nonmetal interfaces

Yan Wang,[1] Xiulin Ruan,[1,*] and Ajit K. Roy[2]

[1]*School of Mechanical Engineering and the Birck Nanotechnology Center, Purdue University, West Lafayette, Indiana 47907, USA*

[2]*Materials and Manufacturing Directorate, Air Force Research Laboratory, Wright Patterson Air Force Base, Dayton, Ohio 45433, USA*

(Received 12 February 2012; published 10 May 2012)

We have used a two-temperature nonequilibrium molecular dynamics method for predicting interfacial thermal resistance across metal-nonmetal interfaces. This method is an extension of the conventional nonequilibrium molecular dynamics for the dielectric-dielectric interface, where a temperature bias is imposed and the heat current is derived. We have included the electron degree of freedom for the interfacial thermal transport problem by treating the electron-phonon coupling with the two-temperature model. The method is demonstrated on two model systems, that is, silicon-copper interface and carbon-nanotube–copper interface. Temperature nonequilibrium between electrons and phonons in the metal side is quantitatively predicted, and a temperature drop across the interface is observed. The results agree with experimental data better than those obtained from conventional nonequilibrium molecular dynamics simulations where only phonons are considered. Our approach is capable of taking into account both the electron and lattice degrees of freedom in a single molecular dynamics simulation and is a generally useful tool for modeling interfacial thermal transport across metal-nonmetal interfaces.

DOI: 10.1103/PhysRevB.85.205311 PACS number(s): 73.40.Ns, 05.70.Np, 68.35.Md, 73.40.−c

I. INTRODUCTION

As the system size drops to micro- or nanoscale, thermal transport across interfaces usually dominates the overall heat transport characteristics. The minimization of chip-package interfacial thermal resistance (R_I) has thus been the major challenge in thermal management of micro/nano electronic devices.[1] Understanding the mechanism of interfacial thermal transport across various dissimilar materials is of fundamental importance to the development of thermal interface materials (TIMs),[1] superlattices,[2] very large scale integrated circuits (VLSICs),[3] etc.

Theoretical approaches such as acoustic mismatch model (AMM)[4,5] and diffuse mismatch model (DMM)[5] correspond to the upper and lower bounds of R_I and can reach reasonable agreement with experiments at temperatures below 40 K (Ref. 5). Sophisticated modifications[3,6–8] to the original models have been proposed for conditions at higher temperatures, but usually rely on a large database of measured material properties as input or introduce fitting parameters to reproduce the experimental data, which has raised doubt that the improved agreement might be fictious.[9] Atomic-level methods such as nonequilibrium Green's function (NEGF) method[10,11] and equilibrium/nonequilibrium molecular dynamics (MD) simulations[9,12–15] have also been extensively used to calculate R_I for various interfaces. Both NEGF and MD simulations only need equilibrium lattice structure and interatomic potential as inputs, and phonon properties such as density of states, dispersion relations[16] and phonon transmittance[17] exist naturally. In modeling inelastic phonon scattering, the NEGF method is usually limited to low-dimensional systems due to its high computational cost.[9] MD simulations can model such effect as well as other complicated conditions such as the atomic reconstruction at the interface straightforwardly,[18] which is not as easily and accurately accessible by other methods. Of course, MD method also has drawbacks such as finite size effect[19] and quantum effect,[20] which can usually be circumvented or minimized with proper simulation domain design and quantum correction to the simulation results. However, all the above methods have only accounted for phononic thermal transport, while ignoring the contribution of electrons. Such simplification is restricted to be valid only for interfaces composed of dielectric and certain semiconductor materials, where electrons contribute much less than phonons to heat transfer. When metals, semimetals, or heavily doped semiconductors are involved, the electronic contribution to heat conduction has to be included.

One approach to conveniently include electron-phonon coupling is the two-temperature model (TTM), which designates electron and phonon as two separate subsystems and assigns a temperature for each.[21–25] Majumdar and Reddy used this model to show that electron-phonon coupling could be an important issue in metal-nonmetal interfaces[21] where relatively dense electron gas is present. Compared to those phononic methods mentioned above, more energy transport channels such as electronic thermal transport and electron-phonon interactions are added, leading to better approximation[21] to realistic energy transport events in materials where electrons are important. To date, TTM, combined with MD, has been used to study nonequilibrium, transient processes such as short pulse laser melting,[23,26] cascade radiation-induced defects, displacement,[27,28] etc., which demonstrated that the incorporation of electrons could often generate significant deviations from what was predicted by MD alone. For the purpose of modeling interfacial thermal transport, TTM has so far been used qualitatively to analyze the contribution of electrons,[21] while TTM alone cannot model thermal interface resistance due to phonons. An approach that can quantitatively include electron and phonon is needed for modeling interfacial thermal transport across metal-nonmetal interfaces.

In this work, we use a two-temperature nonequilibrium MD method, through a combination of TTM and MD, to effectively simulate thermal transport across metal-nonmetal interfaces. We first derive an analytical solution to 1D steady-state heat conduction across metal-nonmetal system, of which the

two ends are maintained at different prescribed temperatures (Dirichlet boundary condition). An exact expression of thermal resistances is obtained. Then we describe the two-temperature MD approach, in which phonon transport is modeled using MD and electron transport is modeled using the finite difference method. This approach achieves simultaneous modeling of phonons and electrons in a single simulation and captures electron-phonon nonequilibrium successfully. This approach is then demonstrated via two case studies: Si-Cu and carbon nanotube (CNT)-Cu interfaces. Our work demonstrates the importance of electron-phonon coupling to the accurate prediction of thermal transport across metal-nonmetal interfaces, which leads to better agreement with experimental data than phononic MD alone.

II. THEORY

A. Two-temperature model

As mentioned above, TTM depicts the coupled electronic and phononic thermal transport in a quite simple picture, through separated temperature fields and a shared coupling term.[22,29–31] The temporal and spatial evolution of temperature fields in this model can be generalized to two coupled heat diffusion equations as shown below:

$$\rho_e c_e \frac{\partial T_e}{\partial t} = \nabla \cdot (\kappa_e \nabla T_e) - g_{ep}(T_e - T_p) + \rho_e r_e, \quad \text{(1a)}$$

$$\rho_p c_p \frac{\partial T_p}{\partial t} = \nabla \cdot (\kappa_p \nabla T_p) + g_{ep}(T_e - T_p) + \rho_p r_p, \quad \text{(1b)}$$

where ρ, c, T, and κ denote the density, specific heat, temperature field, and thermal conductivity of electrons (subscript e) or phonons (subscript p). g_{ep} is the electron-phonon coupling parameter, which will be discussed in the following section. r is a mass normalized source term, including all the external sources of energy exchange/transition events such as the effects of electronic stopping,[22] laser cooling/heating,[23] Peltier cooling/heating, Joule heating, etc.

Equation (1) has been used extensively to describe transient processes such as laser melting or radiation damage or to capture the strength of electron-phonon coupling in metals.[32] A few attempts[21,33,34] have been made to utilize the TTM scheme to determine the electronic contribution to the interface resistance. In order to gain a both qualitative and quantitative insight into the importance of TTM to this topic, we also start with an analytical derivation of a one dimensional (1D) interfacial thermal transport problem with Dirichlet boundary condition (prescribed boundary temperatures), which is usually used in nonequilibrium MD simulations.[35]

The representative temperature profiles for thermal transport across a metal-nonmetal interface are shown in Fig. 1. l denotes the length of the left side (subscript L) or right side (subscript R), which are metal and nonmetal, respectively. T_L and T_R are prescribed temperatures at the left and right end, which form the Dirichlet boundary conditions for this heat transfer problem. T with subscripts n (phonons in the nonmetal side), p (phonons in the metal side), e (electrons in the metal side), and fit (the linear fit of the temperature profile of the electron-phonon equilibrium region) denote corresponding temperature field as a function of position, x. Herein we assume that electrons in the nonmetal side do not

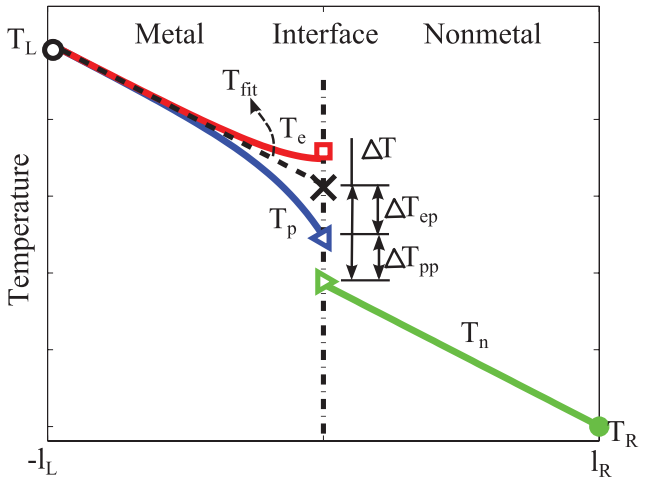

FIG. 1. (Color online) Representative temperature profiles in TTM for a metal-nonmetal interface. T_n, T_p, and T_e are temperature profiles for phonons in the nonmetal side, phonons in the metal side, and electrons in the metal side. T_{fit} is a linear fit of the temperature profile of the electron-phonon equilibrium region. In the metal side near the interface, electrons and phonons have different temperature, which indicates electron-phonon nonequilibrium. ΔT_{ep} and ΔT_{pp} denote the temperature discontinuity related to the electron-phonon coupling in the metal side and the phonon-phonon coupling across the interface, respectively. $\Delta T = \Delta T_{ep} + \Delta T_{pp}$ is the total temperature jump at the interface.

contribute to heat conduction, so that electronic heat transfer is confined in the metal side only. This assumption is reasonable considering that electrons account for only ~0.02% of the overall thermal transport in Si (Ref. 25) and less than ~10% even in metallic single-walled CNTs at room temperature.[36] We are not addressing the term, r, in Eq. (1), which accounts for electronic stopping effects, laser heating/cooling, etc., since they are not within the scope of this work but can be easily implemented in this TTM-MD method if accurate models for these processes are available. Consequently, for 1D steady-state heat transport with constant values of κ_e, κ_p, we obtain the electron/phonon energy diffusion equations coupled via the electron-phonon coupling term, g_{ep}:

$$\frac{d^2 T_e}{dx^2} - \frac{g_{ep}(T_e - T_p)}{\kappa_e} = 0, \quad \text{(2a)}$$

$$\frac{d^2 T_p}{dx^2} + \frac{g_{ep}(T_e - T_p)}{\kappa_p} = 0. \quad \text{(2b)}$$

Equations (2a) and (2b) are essentially the same as the starting equations in Ref. 21. Subtracting Eq. (2a) from Eq. (2b),

$$\frac{d^2 \theta}{dx^2} - \gamma^2 \theta = 0, \quad (3)$$

where $\theta = T_p - T_e$ and

$$\gamma = \sqrt{g_{ep}\left(\frac{1}{\kappa_e} + \frac{1}{\kappa_p}\right)}. \quad (4)$$

Note that the boundary condition at the far end of the metal is $\theta|_{x \to -\infty} = 0$. The solution to Eq. (3) is thus $\theta = c \cdot \exp(\gamma x)$,

where c is a constant of integration to be determined. Accordingly, $\nabla\theta|_{x=0} = \gamma \cdot c$.

Let us denote the steady-state heat current resulting from the temperature bias, $T_L - T_R$, as J, which is positive for left-to-right direction and vice versa. Recall that J is assumed to be carried by both electrons and phonons in the metal side and only by phonons in the nonmetal side; thereby, we have another set of boundary conditions at the interface, which are $-J = \kappa_n \nabla T_n|_{x=0} = \kappa_p \nabla T_p|_{x=0}$ and $\nabla T_e|_{x=0} = 0$, and hence,

$$\nabla\theta|_{x=0} = \nabla T_p|_{x=0} - \nabla T_e|_{x=0} = \nabla T_p|_{x=0} = -\frac{J}{\kappa_p}. \quad (5)$$

We combine $\nabla\theta|_{x=0} = \gamma \cdot c$ with Eq. (5) and get $c = -\frac{J}{\gamma\kappa_p}$, so

$$\theta = -\frac{J}{\gamma\kappa_p}\exp(-\gamma|x|). \quad (6)$$

Equation (6) enables us to define a nonequilibrium length, or cooling length,[33] which quantifies the electron-phonon nonequilibrium distance. Specifically, if we define such a characteristic length as the distance between the position of $\theta_{\max}$ and $5\%\theta_{\max}$, then

$$l_{NE} \approx \frac{3}{\gamma} = \frac{3}{\sqrt{g_{ep}\left(\frac{1}{\kappa_e} + \frac{1}{\kappa_p}\right)}}. \quad (7)$$

In metal, the overall Fourier's law considering both electrons and phonons is

$$-J = \kappa_p \nabla T_p + \kappa_e \nabla T_e \quad (8)$$

and from Eq. (6), we know

$$\nabla\theta = \nabla T_p - \nabla T_e = -\frac{J}{\kappa_p}\exp(\gamma x). \quad (9)$$

Combining Eqs. (8) and (9), it is easy to solve for ∇T_p and ∇T_e. Integrating the results with the Dirichlet boundary conditions, we obtain the exact temperature field in the metal side,

$$T_e = \frac{J}{\kappa_e + \kappa_p}\left[\frac{1}{\gamma}\exp(\gamma x) - \frac{1}{\gamma}\exp(-\gamma l_L) - x - l_L\right] + T_L, \quad (10a)$$

$$T_p = \frac{J}{\kappa_e + \kappa_p}\left[\frac{1}{\gamma}\exp(\gamma x) - \frac{1}{\gamma}\exp(-\gamma l_L) - x - l_L\right] + T_L - \frac{J}{\gamma\kappa_p}\exp(\gamma x). \quad (10b)$$

As a first approximation, we assume that thermal transport across metal-nonmetal interface is only contributed by phonon-phonon coupling, that is, phonon-mediated. Such assumption is commonly adopted in theoretical methods such as DMM and AMM. However, a refined model would consider the penetration of electrons into the nonmetal side, which will be considered in our future work. We define the interfacial thermal conductance caused by such phonon-phonon coupling as h_{pp}, and, correspondingly,

$$\frac{J}{(T_p - T_n)|_{x=0}} = h_{pp}. \quad (11)$$

On the nonmetal side, the Fourier's law is

$$\kappa_n \nabla T_n = -J. \quad (12)$$

With one boundary condition as $T_n|_{x=l_R} = T_R$, Eq. (12) leads to

$$T_n|_{x=0} = T_R + \frac{J \cdot l_R}{\kappa_n}. \quad (13)$$

Combining Eqs. (10), (11), and (13), we finally get

$$R_{\text{tot}} = \frac{T_L - T_R}{J} = \frac{l_L}{\kappa_e + \kappa_p} + \frac{1}{h_{pp}} + \left(\frac{\kappa_e}{\kappa_e + \kappa_p}\right)^{\frac{3}{2}}\left(\frac{1}{g_{ep}\kappa_p}\right)^{\frac{1}{2}} + \frac{l_R}{\kappa_n}. \quad (14)$$

Evidently, Eq. (14) indicates that the metal-nonmetal system can be described as a series thermal circuit. More specifically, the first and the last term on the right-hand side of Eq. (14) are the formal Fourier thermal resistance of the metal and nonmetal segments, respectively. The second and third terms are the interfacial thermal resistances associated with phonon-phonon coupling (R_{pp}) and electron-phonon coupling (R_{ep}), respectively. Our result is essentially the same as Majumdar and Reddy's work,[21] though for different boundary conditions. Subtracting the two bulk thermal resistances, it is evident that the interfacial thermal resistance can be written as

$$R_I = \frac{\Delta T}{J} = R_{pp} + R_{ep} = \frac{1}{h_{pp}} + \left(\frac{\kappa_e}{\kappa_e + \kappa_p}\right)^{\frac{3}{2}}\left(\frac{1}{g_{ep}\kappa_p}\right)^{\frac{1}{2}}. \quad (15)$$

where $\Delta T = (T_n - T_{\text{fit}})|_{x=0}$ and is indicated in Fig. 1 as the summation of ΔT_{ep} and ΔT_{pp}, corresponding to the interfacial temperature discontinuity related to electron-phonon coupling in the metal side and phonon-phonon coupling across the interface, respectively.

B. Input parameters

In practice, the utilization of TTM is usually quite cumbersome due to its input parameters, that is, c_e, κ_e, and g_{ep}. Lin *et al.* conducted comprehensive studies on the temperature dependence of c_e for eight representative metals from first principle,[37] and a linear relation between c_e and T_e is usually valid for a temperature below 1000 K, a regime for most thermal interface applications. κ_e can be approximated via the Wiedemann-Franz law based on a knowledge of the Lorenz number and electrical conductivity, given that most electron-electron collisions are elastic, which has been adopted in previous TTM works.[25,28] Another way to calculate κ_e, as stated in Ref. 37, is through the Drude model, which does not guarantee better approximations due to the complicated temperature dependence of c_e and electron-phonon and electron-electron scattering rates.[37] Tremendous efforts have been made in search of an accurate model of electron-phonon interactions in various materials.[22,26,32,37–41] Duffy and Rutherford divide electron-phonon interactions, through a cutoff ion velocity,[22,40] into two distinct regimes,[42] that is, electronic stopping and electron-phonon coupling. The former regime is characterized by ballistic movement of ions with extremely high energy, for example, 8.6 eV for Fe (Ref. 22), which is not present in most interfacial thermal transport problems. On the other hand, electron-phonon coupling dominates the overall electron-phonon interactions

TABLE I. g_{ep} for Cu obtained via various methods.

Reference	Method	g_{ep} (10^{16} W/m^3 K)
37	*Ab initio*	~5.5[a]
38	Pump-probe experiment through time-resolved transmissivity	
43	*Ab initio*	8.43
32	Pump-probe experiment through transient thermo-reflectance spectroscopy	26[b]

[a]This value is for $T_e = 300$ K. They have obtained g_{ep} for a wide span of T_e up to 2×10^4 K.
[b]This value is for $T_e = 300$ K. $g_{ep} = 8.6 \times 10^{16}$ at $T_e = 100$ K.

in a solid-state crystal, where atoms vibrate around their equilibrium positions. Various methods[32,37,38,43] have been applied to calculate the electron-phonon coupling coefficient, g_{ep}, as a linear approximation of electron-phonon energy exchange through the $g_{ep}(T_e - T_p)$ term in TTM. However, the obtained g_{ep}'s can vary by an order of magnitude for the same material (see Table I for a list of measured g_{ep} for Cu), which suggests the inaccuracy, to a certain extent, of the linear approximation.

III. SIMULATION DETAILS AND RESULTS

A. TTM-MD simulation

For the purpose of thermal transport modeling, MD simulation is advantageous with respect to other theoretical approaches, for example, AMM and DMM, in modeling thermal transport processes in that it naturally includes the effects of interface bonding and topography, without sophisticated assumptions on those properties. The only inputs needed by MD simulation are the atomic structure and empirical interatomic potentials. MD simulations have been used extensively to compute thermal boundary conductance (resistance) across solid-solid interfaces,[9,44,45] however, mainly limited to nonmetals. To incorporate electronic effects into the modeling of radiation damage simulations, Duffy and Rutherford introduced a TTM-MD simulation scheme capable of accounting for electron-phonon coupling, electronic stopping, and both the temporal and spatial evolution of the phononic and electronic subsystems.[22,40] Subsequently, Phillips and Crozier modified Duffy and Rutherford's design to an energy-conserving version by adding a communication process between the electronic and atomic subsystems.[31] Herein we adopt Phillips and Crozier's version, using the LAMMPS package[46] (we have modified its *ttm* module to support nonperiodic boundary conditions), to perform nonequilibrium MD simulation for phonon degree of freedom, which is coupled with finite difference (FD) calculation for the electron degree of freedom.

In parallel with Eqs. (1a) and (1b), the TTM-MD simulation models coupled electronic subsystem and phononic subsystem simultaneously, as illustrated in Fig. 2. Phononic heat diffusion [Eq. (1b) except the last term] is still modeled by the usual MD technique. κ_p is thus calculated implicitly by MD, where its dependence on temperature, interface atomic reconstruction,[18] and mixing[7] are included. In addition, in

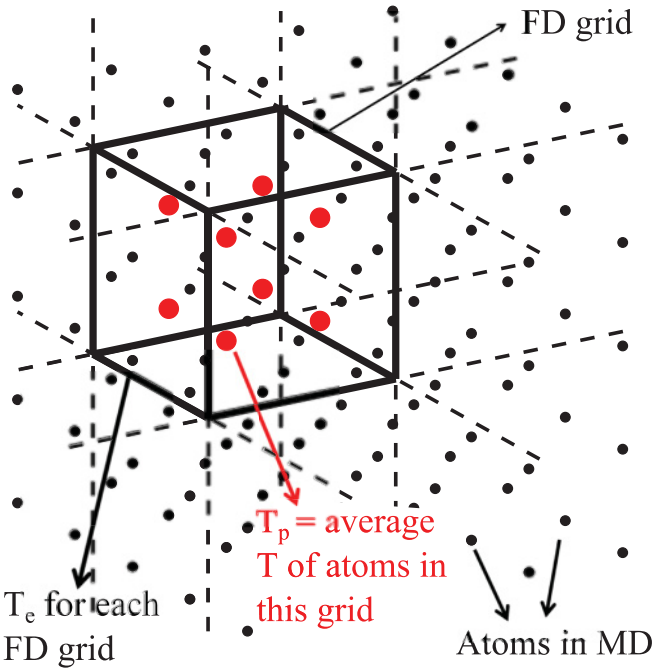

FIG. 2. (Color online) Illustration of the coupled electronic and phononic subsystems using FD and MD in TTM-MD simulations. Lines represent FD grids, with solid ones denoting the grid of interest. Dots are atoms in MD simulations, with enlarged ones denoting the atoms inside the FD grid of interest. Thermal transport in the electronic subsystem is modeled by solving Eq. (1a) using FD method, where each grid has its own T_e, and T_p is the average temperature of the MD atoms inside this grid. The phononic subsystem is modeled by the MD simulation, with each atom subject to a Langevin force, which equilibrates their temperatures to the T_e of the overlapping FD grid.

the TTM-MD approach, electron-phonon nonequilibrium near the interface leads to phonon generation, which can disturb the original phonon scattering, and hence affects phonon transport. This feature is neglected in Majumdar and Reddy's analytical treatment,[21] where κ_p was calculated elsewhere. The electronic subsystem is modeled by solving Eq. (1a) iteratively with the FD method. Phonons and electrons are coupled via the $g_{ep}(T_e - T_p)$ term in Eq. (1), where T_e is the electron temperature of each FD grid, and T_p is the average temperature of the MD atoms inside that grid.

In practice, the equation of motion for an atom i in the MD part is in the form of a Langevin thermostat[22,28,40]:

$$m_i \frac{\partial \mathbf{v}_i}{\partial t} = \mathbf{F}_i(t) - \gamma_i \mathbf{v}_i + \tilde{\mathbf{F}}_i(t), \tag{16}$$

where m and $\mathbf{v}$ are merely the atomic mass and velocity. $\mathbf{F}_i$ is the total force exerted on atom i, evaluated via empirical interatomic potentials. γ_i is a friction term representing the energy loss by electron-ion interactions and is directly related to g_{ep} as[22]

$$\gamma_i = \frac{m_i g_{ep}}{3 n_i k_B}, \tag{17}$$

with n denoting the atom number density and k_B the Boltzmann constant. $\tilde{\mathbf{F}}_i(t)$ is a random force term commonly seen in

Langevin dynamics and, for this specific case,

$$\tilde{\mathbf{F}}_i(t) = \sqrt{\frac{24k_B T_e \gamma_i}{\Delta t}}\tilde{\mathbf{R}}_i, \tag{18}$$

where Δt is the temporal interval of the simulation and $\tilde{\mathbf{R}}$ is a random vector $[R_1, R_2, R_3]$ with $R_j \in [-0.5, 0.5]$. The summation of the last two terms of Eq. (16), that is, $-\gamma_i \mathbf{v}_i + \tilde{\mathbf{F}}_i(t)$, equilibrates the electronic and phononic subsystems to a shared temperature.[22,31]

So far, we have gone through a complete process of the evolution of the phononic subsystem in the MD part. The total energy transferred from the electronic subsystem to the phononic one through the Langevin force, $-\gamma_i \mathbf{v}_i + \tilde{\mathbf{F}}_i(t)$ in Eq. (16), is thus[28,31]

$$\tilde{E}_{ep} = [-\gamma_i \mathbf{v}_i + \tilde{\mathbf{F}}_i(t)]\mathbf{v}_i \Delta t. \tag{19}$$

Finally, we replace $g_{ep}(T_e - T_p)$ with $\tilde{E}_{ep}$ in Eq. (1a), establishing a complete electronic thermal diffusion process, and the total energy of the whole system is also conserved. It should be noted that the validity of both the MD simulation and the FD calculation of electronic heat diffusion is based on the assumption of local equilibrium. To satisfy this criteria, the number of atoms accounted for by each grid should be larger than a critical value to make sure the fluctuation of temperature is small enough, which is in contrast to the discrete nature of FD which prefers finer grids. We have checked our simulations on Si-Cu and CNT-Cu systems, and the temporal local temperature fluctuation is usually below 15% when each grid contains more than 1000 atoms. To successfully model interfacial thermal transport processes, where electron-phonon nonequilibrium adjacent to the interface is crucial, we should also make sure that the FD grids should be sufficiently shorter than l_{NE} in the heat flow direction, as defined by Eq. (7).

B. Case studies

1. *Pure copper*

To verify that this TTM-MD method is capable of modeling coupled electronic and phononic thermal transport in metals, we first calculate the thermal conductivity of a homogeneous Cu ($m_{\mathrm{Cu}} = 63.55$ g/mol, and $\sim 72 \times 4 \times 4$ nm) in the [100] direction, as shown in Fig. 3(a). We do not consider its natural abundance (69.15% ^{63}Cu and 30.85% ^{65}Cu) here since the corresponding mass disorder is negligible in terms of thermal transport. In the MD domain, the outermost layer of atoms on both ends of the Cu are fixed, while the periodic boundary condition is applied to the lateral directions. The FD calculation contains $100 \times 1 \times 1$ girds, which corresponds to 600 atoms/grid. This ensures a temperature fluctuation in each FD grid less than 10%, which is well compatible with the local equilibrium requirement. Adiabatic thermal boundary condition is used at the two ends of the FD domain, which allows for the establishment of a steady temperature gradient. The embedded-atom method (EAM)[47] is adopted for Cu-Cu interactions. The system is first relaxed in the NVT ensemble (300 K) via the Nosé-Hoover thermostat[48,49] for 0.5 ns with a time step of 0.5 fs. After that, the system is switched to nonequilibrium MD, where atomic temperatures at the two ends are maintained at 350 K and 250 K, respectively, through a direct velocity scaling algorithm implemented in LAMMPS.

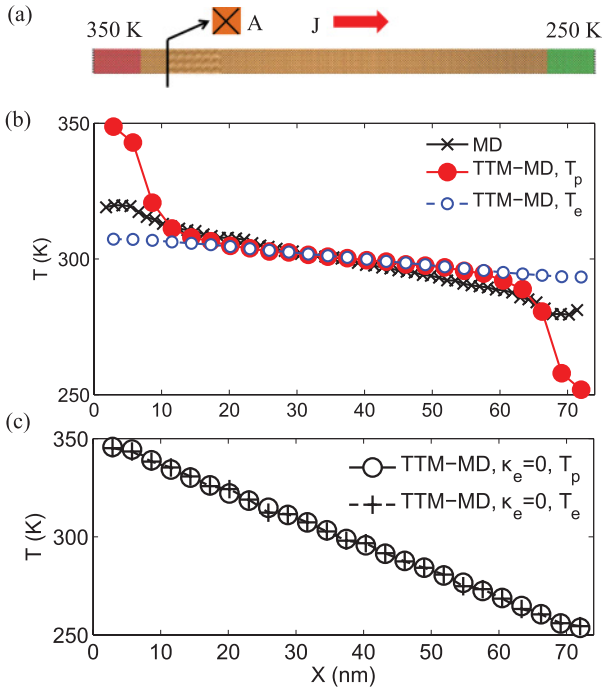

FIG. 3. (Color online) (a) The simulation setup. (b),(c) The steady-state temperature profiles obtained in conventional MD and TTM-MD simulations on pure Cu. Electron-phonon nonequilibrium can be seen at and near the thermostat region in (b). Electron and phonon are always in equilibrium in (c) since we use $\kappa_e = 0$.

The resulting heat current J is calculated by $J = (J_L - J_R)/2$, where J_L and J_R are the amount of kinetic energy injected into the left and right thermostat per unit time. Such nonequilibrium MD simulation is continued for 9×10^6 steps, of which the last 4.5×10^6 steps are used for data production and postprocessing.

We conduct both conventional MD and TTM-MD, and in the latter case we use $\kappa_e = 401$ W/m K, which is actually the total κ of Cu at room temperature. Since the lattice contribution to thermal transport in Cu is rather small compared with the electronic part, previous studies[32] usually used the total κ as a first approximation for κ_e. Besides, we use the value of 2.6×10^{17} W/m^3 K, as obtained from Eesley's experiment, for g_{ep}. The corresponding steady-state temperature profiles are plotted in Fig. 3(b). The temperature gradient $\partial T/\partial x$ can be extracted from the central part of the temperature profiles, where they are linear for both methods and $T_e = T_p$ for TTM-MD. The two electron-phonon nonequilibrium regions near the thermostats are due to the fact that we only apply thermostats to phonons in the TTM-MD simulation, which does not violate the validity of this method as long as we calculate κ with the linear temperature profile in electron-phonon equilibrium region (central part of the structure). As a verification for this method, we also perform TTM-MD with $\kappa_e = 0$, corresponding to $l_{NE} = 0$ from Eq. (7). In the resulting temperature profile [Fig. 3(c)], electrons and phonons have the same temperature all the way from the hot thermostat to the cold one, indicating excellent agreement between our TTM-MD simulation and the analytical solution. Thermal conductivity, κ, is obtained according to the Fourier's law

TABLE II. κ of Cu obtained via different methods.

Source	Method	κ (W/m K)
Ref. 50	Experiment	~401
Ref. 51	Equilibrium MD	~15
Ref. 52	Nonequilibrium MD	~10.4
This work	Nonequilibrium MD	13.6 ± 1.4
This work	TTM-MD	415 ± 11

of heat conduction:

$$\kappa = -\frac{J/A}{\partial T/\partial x}, \tag{20}$$

where A is the cross-sectional area of the Cu.

Table II lists the experimental value[50] of κ, and those calculated in previous theoretical studies[51,52] and in this work, using conventional MD and TTM-MD. As can be seen, κ's from conventional MD are below 15 W/m K, which only accounts for the phononic thermal transport. TTM-MD predicts $\kappa = 415 \pm 11$ W/m K, where the electronic contribution is set to be 401 W/m K, and the phonon contribution accounts for the rest, suggesting the capability of this TTM-MD method in accounting for the electronic contribution to κ.

2. Si-Cu interface

The modern integrated circuit (IC) industry relies significantly on Si and Cu as wafers (substrates) or interconnects. The presence of Si-Cu interface is inevitable and plays an increasingly important role in determining the thermal and electrical performance as the dimension of the devices drops to micro- and nanoscale. Herein we perform MD as well as TTM-MD simulations on thermal transport across a system composed of Si (~35 × 5.4 × 5.4 nm) and Cu (~100 × 5.4 × 5.4 nm) in contact via their (100) faces, which are initially separated by 3.15 Å. In the MD part for both methods, we apply the periodic boundary condition to all directions, that is, x, y, and z. The many-body Tersoff potential[53] and EAM[47] are used for Si-Si and Cu-Cu interactions, respectively. Interfacial interactions between Si and Cu atoms are modeled via a Morse-type potential function,[54]

$$U = D_e[e^{-2\alpha(r-r_0)} - 2e^{-\alpha(r-r_0)}], \tag{21}$$

where $D_e = 0.9$ eV, $\alpha = 1.11$ Å^{-1}, and $r_0 = 3.15$ Å, with a cutoff radius of 3.5 Å. Such pair potential function has been adopted previously to study Cu nanocluster diffusion[55] and deposition[54] associated with CNT or Si. The accuracy of this potential in thermal transport prediction has not been validated yet, and here we use it for the purpose of demonstrating the TTM-MD approach. Potential refinement may be needed in the future for accurate prediction for the Si-Cu interface. The system is first relaxed at zero pressure and constant temperature via the Nosé-Hoover thermostat[48,49] for 0.5 ns. Then the outermost 20 Å of atoms on both ends are fixed, as shown in Fig. 4(a), so that phonons cannot transport from one end to the other end of the simulation cell directly across the periodic boundary. In other words, the periodic boundary condition is replaced with the fixed one for the x direction. After that, we designate the regions (~10 nm long) adjacent to the inner boundary of the fixed ends as thermostats and

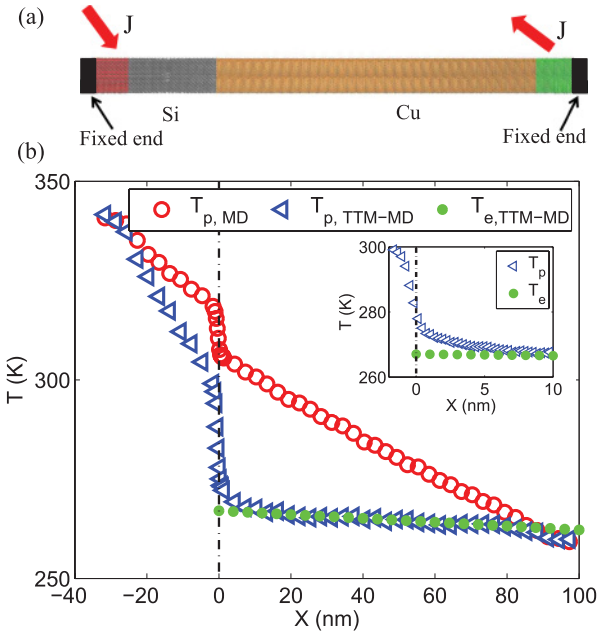

FIG. 4. (Color online) (a) The simulation domain setup, where the segments denoted by different colors are fixed end, hot thermostat, Si system, Cu system, cold thermostat, and fixed end from left to right. (b) The steady-state temperature profiles obtained in conventional MD and TTM-MD simulations on a Si-Cu system. The inset is an enlargement of T_e and T_p adjacent to the interface.

keep injecting a constant heat flux, $J = 3.2 \times 10^{-7}$ W, into one thermostat, while subtracting the same amount from the other simultaneously. We only use FD calculation for the Cu part, instead of the whole structure. The FD domain is divided into $128 \times 1 \times 1$ grids, corresponding to more than 1800 Cu atoms/grid, thus limiting the local temperature fluctuation within 15%.

The steady-state temperature profiles obtained from both conventional MD and TTM-MD simulations are plotted in Fig. 4(b). It should be noted that, to clearly compare these two methods, we apply the Dirichlet boundary condition using the direct velocity rescaling method[46] for this case, with a fixed temperature bias of 80 K, instead of the constant heat flux method we use for all the other simulations in this and following sections. On the Si side, $T_{p,\text{TTM-MD}}$ has much larger slope than $T_{p,\text{MD}}$ since the total heat current is much higher in the former case, due to the addition of electronic thermal transport channel that greatly reduces the thermal resistivity of Cu. On the Cu side, the reduced thermal resistivity of Cu leads to much lower slope of $T_{p,\text{TTM-MD}}$ than $T_{p,\text{MD}}$. The electron-phonon nonequilibrium, of which the analytical form has been shown in Fig. 1, can be clearly seen in the inset of Fig. 4, where T_e is almost flat near the interface, consistent with its adiabatic nature. From the temperature profiles, we can obtain the temperature jump at the interface, ΔT, in the same way as shown in Fig. 1. The interfacial thermal resistance is thus

$$R_I = \frac{A\Delta T}{J}. \tag{22}$$

As discussed in Sec. II B, great caution should be exercised in choosing appropriate input parameters, that is, κ_e, c_e, and

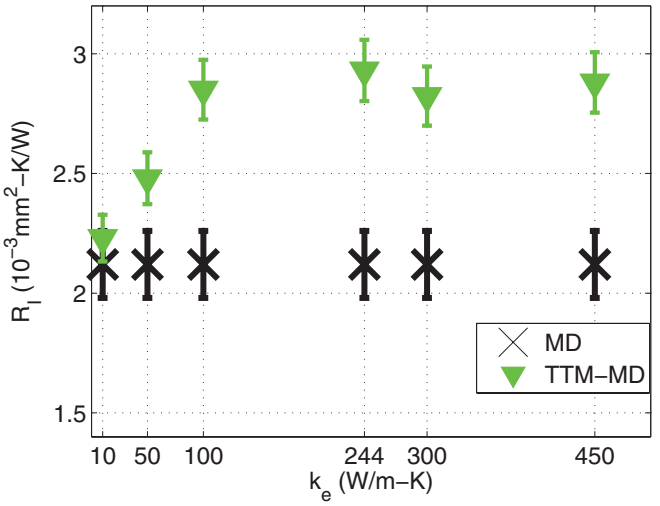

FIG. 5. (Color online) κ_e dependence of R_I predicted by TTM-MD simulations. R_I saturates when $\kappa_e > 100$ W/m K. The data for MD (crosses) are duplicates of the single data obtained from repeated MD simulations at 300 K.

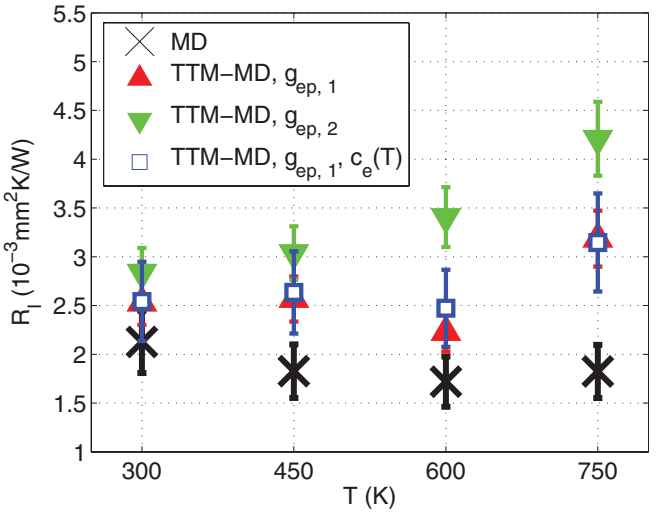

FIG. 6. (Color online) R_I calculated from MD and TTM-MD simulations for Si-Cu interface. $g_{ep,1} = 2.6 \times 10^{17}$ W/m^3 K, and $g_{ep,2} = 5.5 \times 10^{16}$ W/m^3 K. c_e (T) means the use of temperature-dependent volumetric heat capacity C_e (=96.8 J/m^3 K^2 $\times$ T_e) in TTM-MD simulation.

g_{ep}, from many candidates in TTM-MD. However, many metals such as Cu, Au, Pt, and W have fairly constant values of κ in the range of 200 K to 1000 K.[50] Specifically, κ of Cu decreases gradually from 410 W/m K at 200 K to 360 W/m K at 1000 K, where κ_p is only around 10 W/m K[51]. Equation (14) suggests that when $\kappa_e \gg \kappa_p$, R_{ep} is independent of κ_e since $R_{ep} \approx (g_{ep}\kappa_p)^{-0.5}$. As a test, we calculate R_I using κ_e ranging from 10 to 450 W/m K, with constant values of g_{ep} and c_e. As shown in Fig. 5, R_I increases with κ_e at first, but saturates when $\kappa_e > 100$ W/m K. Therefore, in the range of temperature at which we perform TTM-MD simulations on Cu, κ_e has negligible effect on R_I, and we can safely use $\kappa_e = 401$ W/m K for all calculations. Similarly, Eq. (14) reveals that c_e should also be insignificant in steady-state interfacial thermal transport problems. We compare the results using a constant c_e and a temperature dependent c_e (its volumetric form is $C_e = 96.8$ J/m^3 K^2 $\times$ T_e) in Fig. 6 and, evidently, the effect on R_I is minor, as expected.

Lin *et al.* has calculated g_{ep} for various metals including Cu for T_e ranging from room temperature to 2×10^4 K, where g_{ep} is almost constant below 2000 K.[37] Subsequently, Cho *et al.* found better agreement with experimental observation of the temporal evolution of T_e using Lin *et al.*'s data than Elsayed-Ali *et al.*'s. Herein, for the sake of accurate calculation as well as evaluating the importance of g_{ep}, we compute R_I using $g_{ep,1}$ (Ref. 32) $= 2.6 \times 10^{17}$ W/m^3 K, and $g_{ep,2}$(Ref. 37) $= 5.5 \times 10^{16}$ W/m^3 K, respectively. As shown in Fig. 6, $g_{ep,1}$ results in significantly higher (by >25%) R_I than conventional MD, and $g_{ep,2}$ predicts even higher R_I, which agrees with the trend predicted by Eq. (14). Using Eq. (14) with $\kappa_e = 401$ W/m K and $\kappa_p = 13.6$ W/m K (Table II), we can calculate R_{ep} to be $\sim 0.5 \times 10^{-3}$ mm^2 K/W and $\sim 1.1 \times 10^{-3}$ mm^2 K/W for $g_{ep,1}$ and $g_{ep,2}$, respectively. If we simply add R_{ep} to R_{pp} (dark crosses in Fig. 6), which is the method used in Ref. 21, the values are 2.6×10^{-3} mm^2 K/W and 3.2×10^{-3} mm^2 K/W at 300 K, which overpredicts the TTM-MD results by 6% and 15%, respectively. The neglect of electronic effect on phononic thermal transport, by simple summation of R_{pp} and R_{ep} obtained from separate calculations, leads to inherent inaccuracy of previous analytical approaches,[21,33,34] and hence TTM-MD is preferred in that sense.

3. CNT-Cu interface

CNT and graphene, of which both intrinsically possess very high κ and elastic modulus, have been proposed as excellent TIMs[1,56] to fill gaps between solid-solid surfaces, for example, silicon dies, heat sinks, etc. In this section, we conduct TTM-MD simulations on thermal transport across CNT-Cu interface. Similar to Si-Cu, we use the same Morse-type potential function ($D_e = 2.277$ eV, $\alpha = 1.7$ Å^{-1}, and $r_0 = 2.2$ Å)[55] for C-Cu interactions, with a cutoff radius of 2.5 Å. The equilibrium structure is shown in Fig. 7(a), where strong atomic reconstruction of CNT near the interface[18] can be seen due to the rather strong interaction between C and Cu. The zigzag CNT (100.0 nm long and 3.6 nm in diameter) is in end contact with the (100) face of Cu (100 $\times$ 5.4 $\times$ 5.4 nm), with

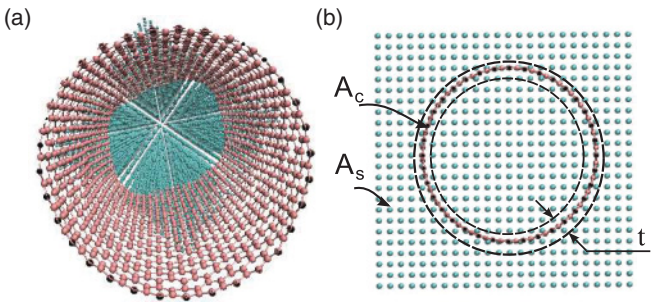

FIG. 7. (Color online) (a) Perspective view (front) of the CNT-Cu interface; (b) schematic of the definition of the cross-sectional area of the Cu substrate (A_s) and the contact (A_c) in Eq. (23).

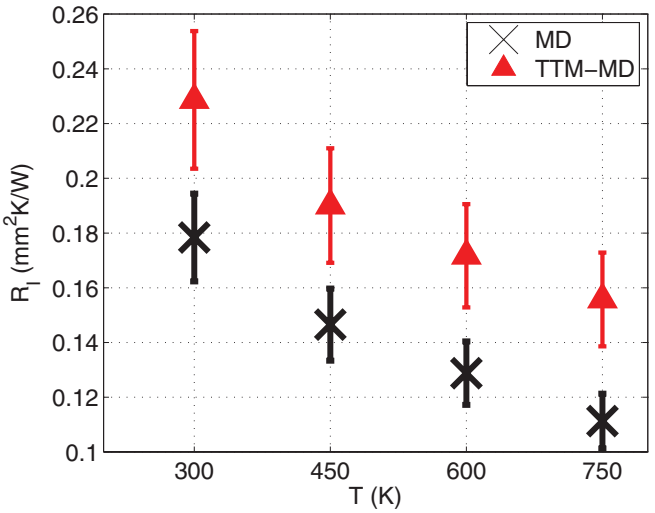

FIG. 8. (Color online) R_I calculated from MD and TTM-MD simulations for the CNT-Cu interface, where $A_c/A_s = 1.0\%$ is used.

an initial separation of 2.2 Å. All the other simulation setup details are the same as our Si-Cu simulations in Sec. III B2.

Special caution should be made to the definition of R_I for CNT-Cu interfaces due to the hollow geometry of CNTs. Herein we calculate R_I of CNT-Cu as the thermal resistance per unit cross-sectional area of the substrate [A_s, see Fig. 7(b)],[13] that is, Cu in this work, which is

$$R_I = \frac{A_s \Delta T}{J} = \frac{A_c \Delta T}{J}\left(\frac{A_s}{A_c}\right), \tag{23}$$

where A_c is the real contact area between CNT and Cu, that is, the annular area of CNT for complete contact conditions. A_c is calculated by $A_c = \pi Dt$, where D and t (0.335 nm) are the diameter and wall thickness of the CNT, respectively. A_c/A_s is usually referred to as the CNT engagement factor.[57] As pointed out in Ref. 57, A_c/A_s is usually between 0.5% and 0.9%, which leads to a large R_I of CNT-metal interfaces. In Ref. 1, the scanning electron microscope image implies that $A_c/A_s \approx 1.89\%$, if we assume that CNTs and the Cu sheet are in complete contact. We calculate R_I for CNT-Cu using a medium value of A_c/A_s, that is, 1.0%.

The temperature dependence of R_I is calculated using both MD and TTM-MD, where $g_{ep} = 5.5 \times 10^{16}$ W/m^3 K and $C_e = 96.8$ J/m^3 K^2 $\times T_e$ are used. As shown in Fig. 8, the TTM-MD predicts higher R_I than MD alone by a factor of ~30% on average. We compare R_I at 300 K calculated by MD and TTM-MD simulations with experimental data in Table III.

TABLE III. Comparison of R_I of CNT-Cu interface from MD, TTM-MD, and experiment.

Source	Method	R_I (mm^2 K/W)
Ref. 1	Experiment[a]	1 ± 0.5
Ref. 1	Experiment[b]	0.9–0.5
This work	Nonequilibrium MD	0.18 ± 0.02
This work	TTM-MD	0.23 ± 0.03

[a]Measure at 0.172 MPa.
[b]Measure at 0.241 MPa.

We should note that if we use $g_{ep} = 2.6 \times 10^{17}$ W/m^3 K, R_I will be ~0.21 mm^2 K/W, which indicates that an accurate value of g_{ep} is crutial to the prediction of R_I.

IV. SUMMARY AND CONCLUDING REMARKS

In this work, we have used TTM-MD simulation to achieve simultaneous modeling of coupled phononic and electronic thermal transport in metal-nonmetal systems in a single simulation. By incorporating the electron degree of freedom to the phononic MD simulation, we are able to capture the nonequilibrium between electron and phonon in a steady-state heat conduction condition, which plays an important role in thermal transport across metal-nonmetal interfaces. The simulation results obtained using this TTM-MD method are physically more sound and are in better agreement with experimental data compared to those obtained using conventional MD simulations.

We also derived the analytical solution for a 1D two-temperature heat conduction problem for general metal-nonmetal systems with Dirichlet boundary condition. The total thermal resistance is proved to be a series summation of the thermal resistances of nonmetal bulk, interfacial phonon-phonon coupling, interfacial electron-phonon coupling, and metal bulk. Compared with conventional MD simulations where only phonons are considered, TTM-MD introduced the interfacial electron-phonon coupling term, which will increase the total interfacial thermal resistance. On the other hand, the addition of the electronic thermal transport channel will reduce the thermal resistance of the metal bulk. Therefore, the overall effect of electrons to a metal-nonmetal interface system depends on which factor dominates, and TTM-MD simulations are thus needed to get more accurate results compared with the analytical solution.

The TTM-MD method in calculating interfacial thermal resistance is generally applicable to many metal-nonmetal interface problems. However, further studies still need to be done to acquire more accurate g_{ep}, κ_e, C_e, and the interatomic potentials between interface atoms. In addition, electrons on the nonmetal side are completely ignored at this moment, which still needs further evaluation of its accuracy. Recent transient thermoreflectance experiments also indicate direct electron-substrate interaction, which is neglected in TTM, as an important thermal transport channel for certain materials with the presence of strong electron-phonon nonequilibrium (very hot electrons).[58] For relatively cold electrons ($T_e \lesssim$ 1000 K), the above effect is much weaker and hence can be rigorously modeled by the current TTM scheme. It should be noted that for the validity of Eq. (22), the simulation domain length of the metal side should be sufficiently longer than the cooling length defined by Eq. (7), so that there can be a linear region with electron-phonon equilibrium to extrapolate for ΔT.

ACKNOWLEDGMENTS

The authors are grateful for support from the Air Force Office of Scientific Research (AFOSR). The authors acknowledge helpful suggestions from Bo Qiu to this work. Y.W. also acknowledges the support from the Graduate School and College of Engineering, Purdue University.

*ruan@purdue.edu

[1] B. A. Cola, J. Xu, C. Cheng, X. Xu, T. S. Fisher, and H. Hu, J. Appl. Phys. **101**, 054313 (2007).
[2] C. Dames and G. Chen, J. Appl. Phys. **95**, 682 (2004).
[3] R. S. Prasher and P. E. Phelan, J. Heat Transfer **123**, 105 (2001).
[4] W. A. Little, Can. J. Phys. **37**, 334 (1959).
[5] E. T. Swartz and R. O. Pohl, Rev. Mod. Phys. **61**, 605 (1989).
[6] P. E. Hopkins, J. Appl. Phys. **106**, 013528 (2009).
[7] T. Beechem, S. Graham, P. Hopkins, and P. Norris, Appl. Phys. Lett. **90**, 054104 (2007).
[8] P. Reddy, K. Castelino, and A. Majumdar, Appl. Phys. Lett. **87**, 211908 (2005).
[9] E. S. Landry and A. J. H. McGaughey, Phys. Rev. B **80**, 165304 (2009).
[10] P. E. Hopkins, P. M. Norris, M. S. Tsegaye, and A. W. Ghosh, J. Appl. Phys. **106**, 063503 (2009).
[11] Z. Huang, T. S. Fisher, and J. Y. Murthy, J. Appl. Phys. **108**, 114310 (2010).
[12] J. Diao, D. Srivastava, and M. Menon, J. Chem. Phys. **128**, 164708 (2008).
[13] A. K. Vallabhaneni, B. Qiu, J. Hu, Y. P. Chen, A. K. Roy, and X. Ruan (unpublished).
[14] L. Hu, T. Desai, and P. Keblinski, Phys. Rev. B **83**, 195423 (2011).
[15] M. Hu, P. Keblinski, J.-S. Wang, and N. Raravikar, J. Appl. Phys. **104**, 083503 (2008).
[16] J. A. Thomas, J. E. Turney, R. M. Iutzi, C. H. Amon, and A. J. H. McGaughey, Phys. Rev. B **81**, 081411 (2010).
[17] P. K. Schelling, S. R. Phillpot, and P. Keblinski, J. Appl. Phys. **95**, 6082 (2004).
[18] S. Shin, M. Kaviany, T. Desai, and R. Bonner, Phys. Rev. B **82**, 081302 (2010).
[19] P. K. Schelling, S. R. Phillpot, and P. Keblinski, Phys. Rev. B **65**, 144306 (2002).
[20] J. E. Turney, A. J. H. McGaughey, and C. H. Amon, Phys. Rev. B **79**, 224305 (2009).
[21] A. Majumdar and P. Reddy, Appl. Phys. Lett. **84**, 4768 (2004).
[22] D. M. Duffy and A. M. Rutherford, J. Phys.: Condens. Matter **19**, 016207 (2007).
[23] Z. Lin, R. A. Johnson, and L. V. Zhigilei, Phys. Rev. B **77**, 214108 (2008).
[24] L. Koči, E. M. Bringa, D. S. Ivanov, J. Hawreliak, J. McNaney, A. Higginbotham, L. V. Zhigilei, A. B. Belonoshko, B. A. Remington, and R. Ahuja, Phys. Rev. B **74**, 012101 (2006).
[25] R. E. Jones, J. A. Templeton, G. J. Wagner, D. Olmsted, and N. A. Modine, Int. J. Numer. Methods Eng. **83**, 940 (2010).
[26] D. S. Ivanov and L. V. Zhigilei, Phys. Rev. B **68**, 064114 (2003).
[27] F. Gao, D. J. Bacon, P. E. J. Flewitt, and T. A. Lewis, Modell. Simul. Mater. Sci. Eng. **6**, 543 (1998).
[28] C. L. Phillips, R. J. Magyar, and P. S. Crozier, J. Chem. Phys. **133**, 144711 (2010).
[29] S. I. Anisimov, B. L. Kapeliovich, and T. L. Perelan, Sov. Phys. JETP **39**, 375 (1974).
[30] A. Caro and M. Victoria, Phys. Rev. A **40**, 2287 (1989).
[31] C. L. Phillips and P. S. Crozier, J. Chem. Phys. **131**, 074701 (2009).
[32] G. L. Eesley, Phys. Rev. B **33**, 2144 (1986).
[33] L. W. da Silva and M. Kaviany, Int. J. Heat Mass Transfer **47**, 2417 (2004).
[34] J. Ordonez-Miranda, J. J. Alvarado-Gil, and R. Yang, J. Appl. Phys. **109**, 094310 (2011).
[35] J. Hu, Y. Wang, A. Vallabhaneni, X. Ruan, and Y. P. Chen, Appl. Phys. Lett. **99**, 113101 (2011).
[36] E. Pop, D. A. Mann, K. E. Goodson, and H. Dai, J. Appl. Phys. **101**, 093710 (2007).
[37] Z. Lin, L. V. Zhigilei, and V. Celli, Phys. Rev. B **77**, 075133 (2008).
[38] H. E. Elsayed-Ali, T. B. Norris, M. A. Pessot, and G. A. Mourou, Phys. Rev. Lett. **58**, 1212 (1987).
[39] B. I. Cho, K. Engelhorn, A. A. Correa, T. Ogitsu, C. P. Weber, H. J. Lee, J. Feng, P. A. Ni, Y. Ping, A. J. Nelson *et al.*, Phys. Rev. Lett. **106**, 167601 (2011).
[40] A. M. Rutherford and D. M. Duffy, J. Phys.: Condens. Matter **19**, 496201 (2007).
[41] M. W. Finnis, P. Agnew, and A. J. E. Foreman, Phys. Rev. B **44**, 567 (1991).
[42] C. P. Race, D. R. Mason, M. W. Finnis, W. M. C. Foulkes, A. P. Horsfield, and A. P. Sutton, Rep. Prog. Phys. **73**, 116501 (2010).
[43] F. Banfi, F. Pressacco, B. Revaz, C. Giannetti, D. Nardi, G. Ferrini, and F. Parmigiani, Phys. Rev. B **81**, 155426 (2010).
[44] H. Zhong and J. R. Lukes, Phys. Rev. B **74**, 125403 (2006).
[45] Z.-Y. Ong and E. Pop, Phys. Rev. B **81**, 155408 (2010).
[46] S. Plimpton, J. Comput. Phys. **117**, 1 (1995).
[47] S. M. Foiles, M. I. Baskes, and M. S. Daw, Phys. Rev. B **33**, 7983 (1986).
[48] S. Nose, J. Chem. Phys. **81**, 511 (1984).
[49] W. G. Hoover, Phys. Rev. A **31**, 1695 (1985).
[50] C. P. Powell and R.W., *Thermal Conductivity of Selected Materials* (US Government Printing Office, Washington, DC, 1966).
[51] B. Feng, Z. Li, and X. Zhang, J. Appl. Phys. **105**, 104315 (2009).
[52] E. B. Webb, J. A. Zimmerman, and S. C. Seel, Math. Mech. Solids **13**, 221 (2008).
[53] J. Tersoff, Phys. Rev. B **37**, 6991 (1988).
[54] Shun-Fa Hwang, Yi-Hung Li, and Zheng-Han Hong, Comput. Mater. Sci. **56**, 85 (2012).
[55] H. J. Hwang, O.-K. Kwon, and J. W. Kang, Solid State Commun. **129**, 687 (2004).
[56] Q. Liang, X. Yao, W. Wang, Y. Liu, and C. P. Wong, ACS Nano **5**, 2392 (2011).
[57] M. A. Panzer, H. M. Duong, J. Okawa, J. Shiomi, B. L. Wardle, S. Maruyama, and K. E. Goodson, Nano Lett. **10**, 2395 (2010).
[58] P. E. Hopkins and P. M. Norris, Appl. Surf. Sci. **253**, 6289 (2007).